

Laser oscillation and thermal lens effect in high-power Nd:YLF laser

Mi Zhou(周密), Ning Wen(温宁), Bo-Xia Yan(颜博霞), Yan-Wei Wang(王延伟), Zhe Han(韩哲), Yuanyuan Fan(范元媛), Qian Wang(王倩), Yan Qi(亓岩)

Citation: Chin. Phys. B.2026. 35(**8**): 084212. DOI: 10.1088/1674-1056/ae2ec0
http://cpb.iphy.ac.cn; http://iopscience.iop.org/cpb

What follows is a list of articles you may be interested in

Dual-wavelength femtosecond Tm:$LuYO_3$ ceramic laser in-band pumped by 1650 nm Er:YAG laser

Jinfang Yang(杨金芳), Purui An(安浦瑞), Chao Bi(毕超), Taotao He(何涛涛), Shichao Yuan(袁诗超), Xinye Tian(田新叶), Man Wan(汪满), Yongle Zhu(朱永乐), Zhong Dong(董忠), and Weijun Ling(令维军)
Chin. Phys. B, 2026, 35 (**7**): 074202. DOI: 10.1088/1674-1056/ae1fe4

Raman lasing and other nonlinear effects based on ultrahigh-*Q* CaF_2 optical resonator

Tong Xing(邢彤), Enbo Xing(邢恩博), Tao Jia(贾涛), Jianglong Li(李江龙), Jiamin Rong(戎佳敏), Yanru Zhou(周彦汝), Wenyao Liu(刘文耀), Jun Tang(唐军), and Jun Liu(刘俊)
Chin. Phys. B, 2022, 31 (**10**): 104204. DOI: 10.1088/1674-1056/ac8728

Unconventional phase transition of phase-change-memory materials for optical data storage

Nian-Ke Chen(陈念科), Xian-Bin Li(李贤斌)
Chin. Phys. B, 2019, 28 (**10**): 104202. DOI: 10.1088/1674-1056/ab3cc3

Wavefront evolution of the signal beam in Ti: sapphire chirped pulse amplifier

Zhen Guo(郭震), Lianghong Yu(於亮红), Wenqi Li(李文启), Zebiao Gan(甘泽彪), Xiaoyan Liang(梁晓燕)
Chin. Phys. B, 2019, 28 (**1**): 014203. DOI: 10.1088/1674-1056/28/1/014203

High power external-cavity surface-emitting laser with front and end pump

Lidan Jiang(蒋丽丹), Renjiang Zhu(朱仁江), Maohua Jiang(蒋茂华), Dingke Zhang(张丁可), Yuting Cui(崔玉亭), Peng Zhang(张鹏), Yanrong Song(宋晏蓉)
Chin. Phys. B, 2018, 27 (**8**): 084205. DOI: 10.1088/1674-1056/27/8/084205

Laser oscillation and thermal lens effect in high-power Nd:YLF laser

Mi Zhou(周密)[1,2], Ning Wen(温宁)[1], Bo-Xia Yan(颜博霞)[1], Yan-Wei Wang(王延伟)[1], Zhe Han(韩哲)[1], Yuanyuan Fan(范元媛)[1], Qian Wang(王倩)[1], and Yan Qi(亓岩)[1,†]

[1] *Institute of Microelectronics of the Chinese Academy of Sciences, Beijing* 100029, *China*
[2] *University of Chinese Academy of Sciences, Beijing* 101418, *China*

(Received 29 October 2025; revised manuscript received 15 December 2025; accepted manuscript online 18 December 2025)

A side-pumped Nd:YLF (yttrium lithium fluoride) laser is investigated to characterize dual-wavelength oscillation and thermal lens effects. An improved method, which involves measuring the waist size and beam quality of the laser under different pump powers and subsequently fitting the data using ABCD matrix propagation formalism, is proposed to measure thermal lens effects in the Nd:YLF crystal for multimode lasers. For π-polarization at 1047 nm, the strong negative thermal focal length along the *a*-axis severely limits its high-power output, while for σ-polarization at 1053 nm, wavelength selection is a dominant factor due to its relatively weak thermal lens effect. Based on this method, the resonator stability of 1047 nm lasing is optimized, and the thermal lens limitation is mitigated by a compensating concave mirror. A maximum single-wavelength oscillation power of 53 W at 1047 nm is achieved with an optical-to-optical conversion efficiency of approximately 24%, which is comparable to that of single-wavelength oscillation at 1053 nm.

Keywords: Nd:YLF, thermal effects, wavelength selection, 1047 nm

PACS: 42.70.Hj, 68.60.Dv, 42.55.Xi, 42.25.Lc

DOI: 10.1088/1674-1056/ae2ec0 **CSTR:** 32038.14.CPB.ae2ec0

1. Introduction

In recent years, the demand for high-power lasers has grown rapidly across various fields, including military applications, industrial manufacturing, scientific research, medical treatments, telecommunications, and environmental monitoring.[1–5] Compared to other Nd^{3+} ion-doped gain crystals, the unique properties of the Nd:YLF (yttrium lithium fluoride) crystal make it particularly promising for meeting the requirements of high-power lasers. Its long fluorescence lifetime and high energy storage capability enable efficient handling of high-power pumping, while its natural birefringence ensures stable and high-quality laser output. Moreover, the negative thermal lens effect of Nd:YLF renders it suitable for high-power and high-energy lasers with repetition rates of several kilohertz, as well as for high-efficiency conversion in various applications.[6–8]

In view of the wide range of applications and the growing demand for high-power lasers, the development of efficient and stable Nd:YLF laser systems is of great importance. Various pumping configurations have been developed to realize high-power Nd:YLF lasers.[9–11] Using two partially end-pumped Nd:YLF slabs in one stable–unstable hybrid resonator, the system delivered a continuous-wave output of 74 W at 1047 nm, and produced pulses of 24.2 mJ and 7.1 ns under Q-switched operation at 1 kHz.[11] The utilization of slab geometries demands complex pump and resonator designs, and Nd:YLF's mechanical brittleness makes slab fabrication especially challenging. In contrast, side-pumped Nd:YLF modules, where the crystal is surrounded by laser diodes, feature a large gain volume that enables more uniform heat dissipation. This reduces peak thermal stress, thereby lowering the risk of fracture and suppressing energy-transfer upconversion processes. Furthermore, side-pumped modules can be cascaded to increase pumping and gain areas, enabling higher-power pumping and the production of high-power lasers with output powers of tens or hundreds of watts or more.

Many studies have been conducted on side-pumped Nd:YLF crystals based on high-power 1053 nm operation, and commercialized laser products have been brought to market.[12–15] A Nd:YLF laser was reported to produce 527 nm pulses exceeding 100 mJ at a 1 kHz repetition rate, with a pulse width of 100 ns and a beam quality factor (M^2) in the range of 10–15.[13] Two orthogonal Nd:YLF series structures, in which three diode bars were arranged at 120° angles around the crystal, were employed to counteract the thermal lens effect, producing an output of 110 W of continuous-wave 1053 nm laser or 51.1 W of pulsed 527 nm laser at repetition rates of 1 kHz.[15]

However, reports of high-power side-pumped 1047 nm lasers remain scarce, possibly attributable to strong thermal astigmatism and susceptibility to stress-induced fracture under high pump intensities. In 1992, a TEM_{00} polarized 40 W beam at 1047 nm was obtained in a Nd:YLF laser by side-pumping with a lamp at 7 kW input power, while the overall efficiency was only 0.54%.[16] A multi-pass slab (MPS) Nd:YLF laser transversely pumped by an 863 nm laser diode (LD) in an

†Corresponding author. E-mail: qiyan@ime.ac.cn

© 2026 Chinese Physical Society and IOP Publishing Ltd. All rights, including for text and data mining, AI training, and similar technologies, are reserved.

astigmatic resonator achieved a maximum continuous-wave output of 29 W in multi-mode operation or 23 W in TEM_{00} mode.[17]

The output characteristics of a high-power side-pumped Nd:YLF laser are investigated, and the thermal lens effects are quantified by establishing a direct correlation between measurable multimode beam parameters. By identifying the thermal lens along the *a*-axis as the primary limitation to 1047 nm operation, we mitigate this effect through resonator optimization and achieve a significant enhancement in output power.

2. Experimental setup

The schematic of the experimental setup is shown in Fig. 1. The side-pumped module features an a-cut Nd:YLF crystal rod with 0.8% doping concentration, 92 mm in length, and 4 mm in diameter, assembled with five LD bars positioned at a 72° angle. The *c*-axis of the crystal is vertical and orthogonal to the rod axis. Taking into account the thermal focal length of the crystal rod, a flat-concave resonator cavity has been designed to maintain stable operation. M1 has a curvature of 1000 mm and exhibits high reflectivity at both 1053 nm and 1047 nm. M2 is a plane mirror and is partially transmissive at wavelengths of 1053 nm and 1047 nm, and the cavity length is approximately 450 mm. A polarizer is used for selecting polarized light. A polarizing beam splitter (PBS) separates the two orthogonally polarized components of the output laser. The component parallel to the *c*-axis is π-light (1047 nm), and the component perpendicular to the *c*-axis is σ-light (1053 nm). A power meter and a beam analyzer are used to measure the power and beam quality of the output lasers, respectively.

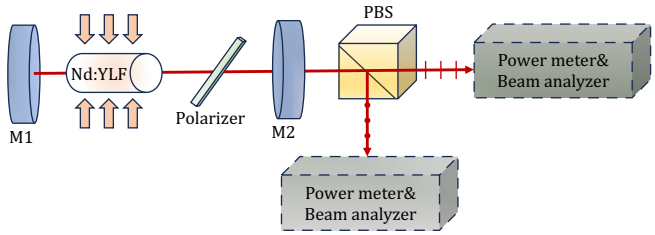


Fig. 1. Schematic of the experimental setup.

According to the absorption spectra of Nd:YLF with 0.8% doping concentration,[18] the crystal exhibits a broad absorption band around 796 nm with strong absorption coefficients for both π- and σ-polarized light. Given the commercial availability of high-power, long-lifetime 796 nm laser diodes, this wavelength was consequently selected for pumping.

Based on the relationship between laser output and cavity parameters, the optimal output coupler transmittance is calculated to lie between 14% and 17%. Accordingly, two output couplers with transmittances of 15% and 20% are employed in the experiments.

3. Results and discussion

Initially, the polarizer is removed, allowing the cavity to directly output a laser with an output coupler of 15% or 20%. The results are depicted in Fig. 2. The 1047 nm laser preferably oscillates with a low threshold and quickly reaches the peak value. Then, it begins to decrease rapidly as the pump power increases. Meanwhile, the 1053 nm laser begins oscillating and soon exceeds the 1047 nm laser, dominating the main portion of the output. This phenomenon, known as dual-wavelength competition, has been observed in many anisotropic gain media, such as Nd:YVO_4,[19] Nd:$GdVO_4$,[20] Nd:$LuVO_4$,[21] Nd:$YAlO_3$,[22] Tm:$LuYO_3$.[23] In our Nd:YLF experiment, the 1047 nm and 1053 nm wavelengths are spectrally close and share similar spectroscopic properties. During the dual-wavelength competition, any proportion of the two wavelengths can be achieved by precisely aligning the cavity. For instance, by adjusting the output coupler with a transmittance of 20%, the power of 1047 nm can vary from nearly zero to its maximum value within the pump power range of 120 W to 200 W, while the 1053 nm laser power correspondingly varies from its maximum to nearly zero. Depending on the pump power, the total power of the two wavelengths appears to be close to a given value. The ability to achieve any ratio of two wavelengths in the dual-wavelength competition through simple cavity adjustments could be very attractive for terahertz (THz) generation.[24]

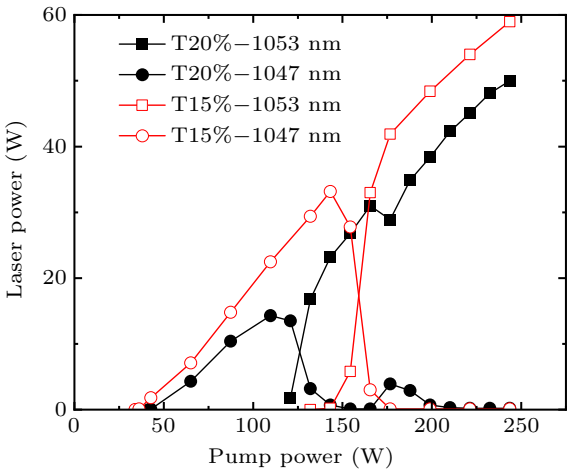


Fig. 2. Output power with the optical coupling of T15% and T20%, respectively.

To avoid fracture of Nd:YLF due to excessive thermal stress under high-power pumping, it is essential to operate within the crystal's thermal limits. The stress fracture threshold of Nd:YLF is approximately 40 MPa,[10,24,25] which corresponds to a maximum allowable absorbed pump power of about 23.34 W per millimeter of crystal length. Therefore, we set the total absorbed pump power to 243 W, well below the fracture limit when distributed over the pumped volume.

As shown in Fig. 2, because the stimulated emission cross section is larger at 1047 nm, its oscillation has a lower threshold for both 15% and 20% transmission output couplers. However, the output of 1047 nm rapidly declines to nearly zero as the pump power increases. This is attributed to the intense competition among ions in the upper level with the other wavelength, as well as a cavity mismatch caused by the strong negative thermal focal length (discussed below). In contrast, despite a higher threshold, the 1053 nm laser gradually dominates the subsequent competition until its competitor drops to zero. Additionally, the 1053 nm laser exhibits nearly linear power scaling with no roll-off, indicating great potential for high-power output.

In Fig. 2, it is obvious that the 15% output coupler performs better than the 20% coupler in terms of laser output, including laser threshold, conversion efficiency, and maximum power, which is consistent with the theoretical calculation. Therefore, the 15% output coupler is chosen for the following experiments. The maximum laser power is 59.1 W under the maximum pump power of 243 W, yielding an optical-to-optical conversion efficiency of 24.3%.

In order to obtain single-wavelength oscillation in the cavity, the polarization selector is typically inserted to select either π- or σ-polarized light. In this case, a horizontal Brewster polarizer is incorporated into the experimental setup near the side-pumped module. The laser power of the selected σ-polarized light is shown in Fig. 3. Due to the insertion loss of the polarizer and the higher threshold for 1053 nm, the overall output power is initially lower, but eventually reaches 58.8 W, which is nearly equivalent to the output power observed in the absence of the polarizer. The slope efficiency of the 1053 nm laser power is 30.9%. The emission spectrum monitored by an optical spectrum analyzer (Ocean Optics USB4000) is displayed in the inset of Fig. 3 and confirms the absence of 1047 nm emission across the entire pump power range, with only 1053 nm lasing observed.

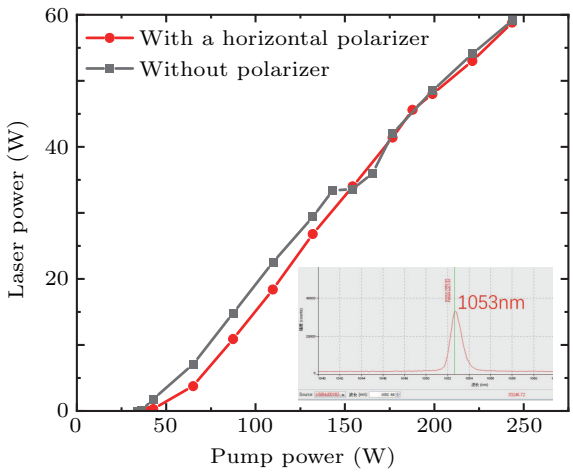


Fig. 3. Output power of 1053 nm with and without the horizonal polarizer. The inset shows the spectrum.

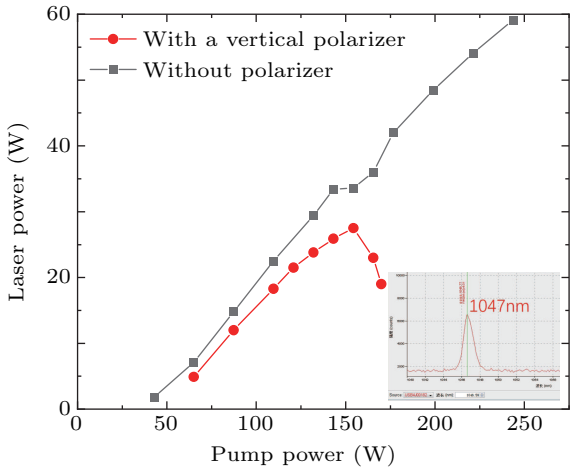


Fig. 4. Output power of 1047 nm with and without the vertical polarizer. The inset shows the spectrum.

When the polarizer is rotated into the vertical direction, single-wavelength oscillation of the π-polarized 1047 nm laser is realized, with the power and spectrum shown in Fig. 4. The difference in output power with and without the polarizer is primarily attributed to the insertion loss of the polarizer. As the pump power increases, the 1047 nm output power rises accordingly but saturates at a maximum of 27.5 W when the absorbed pump power reaches 154 W, after which it drops sharply. This behavior indicates that, unlike the σ-polarized 1053 nm line, the π-polarized 1047 nm transition cannot sustain high-power scaling in this configuration. Since only one wavelength is oscillating, the dual-wavelength competition factor can be excluded, and the decline in laser power is mainly due to cavity mismatch caused by the strong negative thermal focal length of Nd:YLF crystals along the a-axis for π-polarized 1047 nm operation.

The laser crystal can be regarded as being uniformly pumped and subjected to a volume heat source. Therefore, the thermal focal length can be expressed as[26]

$$f = \frac{KA}{P}\left[\frac{1}{2}\frac{\mathrm{d}n}{\mathrm{d}T} + \alpha C_{r,\phi} n_{\mathrm{o}}^3 + \frac{\alpha R(n_{\mathrm{o}}-1)}{L}\right]^{-1}, \qquad (1)$$

where K is the thermal conductivity coefficient of the crystal, A is the area of the cross section of the crystal, $\frac{\mathrm{d}n}{\mathrm{d}T}$ is the temperature coefficient of the refractive index of the crystal, α is the thermal expansion coefficient, R is the radius of the beam waist, L is the length of the crystal, n_{o} is the refractive index of the crystal, P is the total heat load power in the crystal, and $C_{r,\phi}$ is the photo-elastic coefficient.

As stated in Eq. (1), the thermal focal length is mainly composed of three components, namely, the refractive index change caused by thermal stress, the photo-elastic effect, and the focal length change caused by the bulging of the rod end faces. This results in thermal lens astigmatism between the c-axis and the a-axis, which leads to poor laser beam quality. The thermal focal length of the crystal could be obtained by measuring the TEM_{00} mode waist size on the plane output

coupler and then fitting it to the ideal waist calculated from the resonant cavity.[27]

However, this method is not accurate for measuring multimode lasers. Therefore, based on this approach, we propose an improved method to measure the thermal focal length at both 1053 nm and 1047 nm under multimode operation. The method employs a beam analyzer (OPHIR, BSQ-SP920) to simplify the measurement procedure and reduce experimental uncertainty. At various pump powers, the beam waist radius ω_{m} and beam quality factor M^2 are measured separately along the crystal's a-axis and c-axis. Since the resonator is configured as a plano–concave resonator, the beam waist is located at the plane output coupler, making ω_{m} also correspond to the beam radius at this mirror.

As in the case of circular symmetry, the waist and beam divergence of higher-order Gaussian lasers can be denoted as follows:[28]

$$\omega_{pl} = \omega_0 \times \sqrt{2p+l+1}, \tag{2}$$

$$\theta_{pl} = \theta_0 \times \sqrt{2p+l+1}, \tag{3}$$

where p and l are the transverse mode indices of higher-order Gaussian laser modes along two axes, ω_0 and θ_0 are the waist radius and the half angle of divergence of the TEM_{00} mode, ω_{pl} and θ_{pl} are the waist radius and the half angle of divergence of the higher-order mode, respectively.

Based on the equations above, we assume that the waist and beam divergence of each higher-order mode degrade proportionally. Given that the beam quality factor M^2 of a multimode laser is the weighted sum of all higher-order modes, it follows that the weight of each higher-order mode in M^2 would be the same as that in the waist and beam divergence. Therefore, we assume that the waist and beam divergence of a multimode laser deteriorate in equal proportion. Specifically, we introduce a virtual TEM_{00} mode in the cavity whose beam waist ω_2 satisfies

$$\omega_2 \approx \frac{\omega_{\mathrm{m}}}{M}, \tag{4}$$

where ω_{m} is the measured beam waist of the actual multimode output, and $M = \sqrt{M^2}$. This virtual mode serves as a convenient reference for applying Gaussian beam propagation to the effective thermal lens in multimode operation.

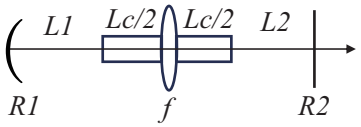


Fig. 5. Equivalent cavity model incorporating the thermal lens.

Therefore, the value of f can be calculated by fitting the waist size of the virtual TEM_{00} mode ω_2 through ABCD matrix propagation formalism. Figure 5 illustrates the equivalent cavity model, in which the thermally induced lensing effect is represented by a thin lens positioned at the center of the Nd:YLF crystal. Taking the output coupler M2 as the reference plane, the round-trip matrix can be written as

$$\begin{bmatrix} A & B \\ C & D \end{bmatrix} = \begin{bmatrix} 1 & L2 \\ 0 & 1 \end{bmatrix} \begin{bmatrix} 1 & \frac{Lc}{2n} \\ 0 & 1 \end{bmatrix} \begin{bmatrix} 1 & 0 \\ -\frac{1}{f} & 1 \end{bmatrix} \begin{bmatrix} 1 & \frac{Lc}{2n} \\ 0 & 1 \end{bmatrix} \begin{bmatrix} 1 & L1 \\ 0 & 1 \end{bmatrix} \begin{bmatrix} 1 & 0 \\ -\frac{2}{R1} & 1 \end{bmatrix} \begin{bmatrix} 1 & L1 \\ 0 & 1 \end{bmatrix} \begin{bmatrix} 1 & \frac{Lc}{2n} \\ 0 & 1 \end{bmatrix} \begin{bmatrix} 1 & 0 \\ -\frac{1}{f} & 1 \end{bmatrix} \begin{bmatrix} 1 & \frac{Lc}{2n} \\ 0 & 1 \end{bmatrix} \begin{bmatrix} 1 & L2 \\ 0 & 1 \end{bmatrix} \begin{bmatrix} 1 & 0 \\ -\frac{2}{R2} & 1 \end{bmatrix}, \tag{5}$$

where $R1$ and $R2$ are the curvatures of mirrors M1 and M2, respectively, $L1$ and $L2$ are the distances from mirrors M1 and M2 to the crystal, respectively, and Lc and n are the length and refractive index of the Nd:YLF crystal, respectively. The Gaussian beam radius ω_2 at mirror M2 is given by

$$\omega_2 = \sqrt{\frac{\lambda}{\pi} \frac{2B}{\sqrt{4-(A+D)^2}}}, \tag{6}$$

where λ is the wavelength of the oscillating laser. Therefore, the thermal focal length of the crystal f can be obtained by fitting Eqs. (5) and (6).

To improve measurement accuracy, the beam radius and beam quality of the multimode laser are recorded in triplicate at each pump power and subsequently averaged before fitting. The fitting results, representing the thermal focal lengths of the crystal along the a-axis and c-axis during 1047 nm (π-polarization) and 1053 nm (σ-polarization) lasing under different pump powers, are plotted in Fig. 6. Due to the sharp drop in laser power for π-polarization, thermal lens measurements are discontinued when the pump power exceeds 170 W. The thermal focal length of the π-polarized 1047 nm laser is strongly negative along the a-axis, reaching approximately -1 m at 160 W pump power as shown in Table 1, while along the c-axis it is less negative, reaching about -2.5 m. Extrapolation suggests that the focal lengths would become more negative with higher pump powers. The anisotropy between the two axes arises primarily from the intrinsic differences in the thermo-optic and photo-elastic coefficients of Nd:YLF, which govern the thermally induced refractive index changes under heat loading.

For σ-polarization at 1053 nm, the thermal focal length is slightly negative along the c-axis, on the order of meters, even when the pump power exceeds 200 W. However, the measured variation of the waist size of the multimode ω_2 along the a-axis fails to exhibit a clear trend across different pump powers. The difficulty in distinguishing and quantifying thermal effects may stem from their being obscured by the simulta-

neous deterioration of beam quality. The thermal lens of the σ-polarized 1053 nm laser along the a-axis is reported to be slightly positive in some studies,[16,25,27,29] which predominantly contributes to the high-power output of 1053 nm.

In order to further study the thermal characteristics of the Nd:YLF crystal and validate the proposed method, the curvature of M1 is changed to 500 mm and 2000 mm, respectively, to obtain higher output power at 1047 nm. The vertical polarizer is maintained in the cavity to ensure π-polarized oscillation. Figure 7 shows the output power of the 1047 nm laser with different curvatures of M1. As can be seen, increasing the curvature of M1 leads to a sharp decline in laser power. With a radius of curvature (ROC) of 2000 mm, the power of the 1047 nm laser drops as the pump power approaches 100 W, at which point the thermal focal length along the a-axis is approximately 2.1 m as shown in Fig. 6.

Table 1. Measured parameters and fitted thermal focal length for π-polarization along the a-axis.

Power (W)	61	72	83	94	106	117	128	140	151	162	174
M^2	5.44	5.21	5.02	4.73	4.56	4.03	3.68	3.40	3.25	3.02	2.96
$2\omega_m$ (μm)	1990	2027	2049	2087	2118	2129	2139	2185	2174	2379	2490
ω_2 (μm)	427	444	457	480	496	530	557	592	603	684	724
fa-π-polarization (m)	−6.6	−4.2	−2.98	−2.24	−1.88	−1.52	−1.35	−1.21	−1.18	−1.03	−0.99

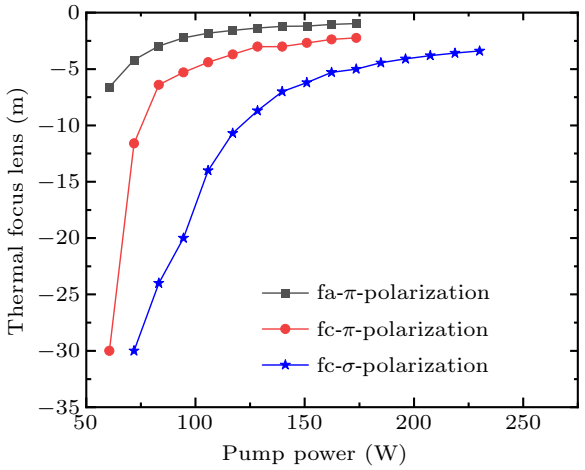


Fig. 6. The thermal focal length for π- and σ-polarization along the a-axis and the c-axis.

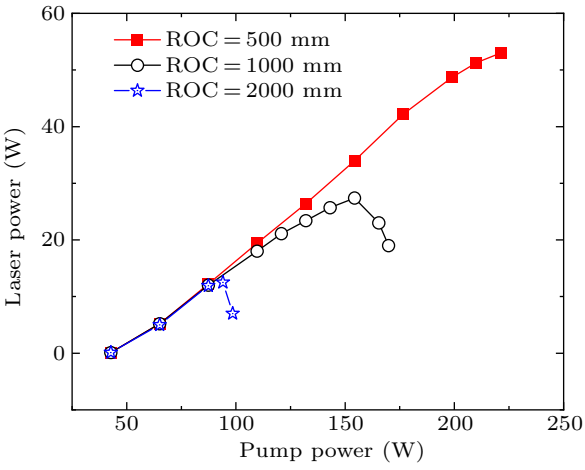


Fig. 7. Laser output power of 1047 nm with different curvature of M1.

When the curvature of M1 is set to 500 mm, it assists in maintaining the thermal stability of the cavity. Consequently, a maximum output power of 53 W for the π-polarized 1047 nm laser is achieved at a pump power of 221 W. The conversion and slope efficiencies of the 1047 nm laser are 24.0% and 30.6%, respectively. These values are comparable to those of the 1053 nm laser with a ROC mirror of 1000 mm in Fig. 3. Furthermore, we demonstrate that the same output power of 53 W at 1047 nm can be realized in the absence of the vertical polarizer. This proves that the cavity curvature can serve as a compensatory mechanism for the thermal effect. Maintaining operation within the thermally governed stable region is essential for single-wavelength lasing at 1047 nm.

4. Conclusion

In summary, this study investigates dual-wavelength operation in high-power, side-pumped Nd:YLF lasers, showing that the power scalability of the 1047 nm line (π-polarization) is predominantly constrained by a strong negative thermal lens along the a-axis. In contrast, the 1053 nm line (σ-polarization), with its comparatively weaker thermal lensing, is governed by wavelength competition. To address this issue, we developed an improved method for quantifying thermal lensing in multimode lasers by linking the thermal focal length to measurable beam parameters (waist size and beam quality factor, M^2) via an ABCD matrix. This method provides a practical approach for resonator design, enabling us to achieve a high-power 53 W output at 1047 nm by implementing a curvature-matched output coupler tailored to compensate for its negative thermal lens. These results establish a practical roadmap for optimizing thermal management and enabling predictable power scaling not only in high-power Nd:YLF lasers but also in other multimode solid-state laser systems.

Acknowledgments

Project supported by the National Key Research and Development Program of China (Grant No. 2023YFB3610901) and the Key Laboratory of Functional Crystals and Laser Technology, Technical Institute of Physics and Chemistry, Chinese Academy of Sciences.

References

[1] Ma Q, Mo H and Zhao J 2018 *Opt. Commun.* **413** 220

[2] Pati B and Rines G A 2012 *Proc. Conf. Lasers Electro-Opt. (CLEO)* (San Jose, CA) pp. 1

[3] Liang H C, Wu C S and Gu S A 2017 *Proc. Laser Congr.* (ASSL, LAC) (Nagoya) pp. JTh2A.20

[4] Bagnoud V, Guardalben M J, Puth J, Zuegel J D, Mooney T and Dumas P 2005 *Appl. Opt.* **44** 282

[5] Polyakov V M, Vitkin V V, Lychagin D I, Krylov A A, Buchenkov V A and Kashcheev S V 2014 *Proc. Int. Conf. Laser Opt.* (St. Petersburg) pp. 1

[6] Murray J E 1983 *IEEE J. Quantum Electron.* **19** 488

[7] Magni V, Cerullo G, Silvestri S D, Svelto O, Qian L J and Danailov M 1993 *Opt. Lett.* **18** 2111

[8] Vanherzeele H 1988 *Opt. Lett.* **13** 369

[9] Zuo Z Y, Dai S B, Zhu S Q, Yin H, Li Z and Chen Z Q 2018 *Opt. Lett.* **43** 4578

[10] Bollig C, Jacobs C, Esser M, Bernhardi E and von Bergmann H 2010 *Opt. Express* **18** 13993

[11] Li D, Ma Z, Haas R, Schell A, Zhu P, Shi P and Du K 2008 *Opt. Lett.* **33** 1708

[12] Armstrong M, Zhu X, Gracewski S and Miller R J D 1999 *Opt. Commun.* **169** 141

[13] Burzo A, Kilmer J and Yin Y 2015 *J. Laser Appl.* **27** S29302

[14] Dai Q, Zhang S C, Li Y Q, Cui J F, Ning R B and Wu R N 2019 *Optik* **176** 655

[15] Pang Y, Xue R, Lu W and Chen Z 2024 *Appl. Opt.* **63** 1572

[16] Cerullo G, De Silvestri S and Magni V 1992 *Opt. Commun.* **93** 77

[17] Pati B and Rines G A 2009 *Proc. Adv. Solid-State Photonics* (Denver, CO) p. WB10

[18] Wetter N, Sousa E, Camargo F, Ranieri I and Baldochi S 2008 *J. Opt.* **10** 104013

[19] Zhou S, Gu P, Li X and Liu S 2017 *Chin. Opt. Lett.* **15** 071401

[20] Pallas F, Herault E, Roux J F, Kevorkian A, Coutaz J L and Vitrant G 2012 *Opt. Lett.* **37** 2817

[21] Huang Y, Cho C Y, Huang Y J and Chen Y F 2012 *Opt. Express* **20** 5644

[22] Lü Y, Zhai P, Xia J, Fu X and Li S 2012 *J. Opt. Soc. Am. B* **29** 2352

[23] Yang J, An P, Bi C, He T, Yuan S, Tian X, Wan M, Zhu Y, Dong Z and Ling W 2025 *Chin. Phys. B* (submitted)

[24] Zhang J, Liu H, Xia J and Fu X 2015 *Chin. Opt. Lett.* **13** 031402

[25] Peng X, Xu L and Asundi A 2005 *Appl. Opt.* **44** 800

[26] Koechner W 2006 *Solid-State Laser Engineering* 6th edn. (New York: Springer) pp. 444

[27] Hardman P J, Clarkson W A, Friel G J, Pollnau M and Hanna D C 1999 *IEEE J. Quantum Electron.* **35** 647

[28] Hodgson N and Weber H 1997 *Optical Resonators* (London: Springer) pp. 171

[29] Zhang Z, Liu Q, Nie M, Ji E and Gong M 2015 *Appl. Phys. B* **120** 689